Analysis and Simulation of High Orbit Weak Signal Tracking Algorithm

Xiaojiang Yang, Qian Yu(✉), and Dongbo Pei

Space Star Technology Company Limited, Beijing 100195, China
yuqian818@126.com

Abstract. Autonomous navigation technology of high orbit spacecraft is one of new aerospace techniques that are badly in need of development in China. It is widely used in communication, navigation, meteorology, early warning and other fields. High orbit navigation receiver provides a convenient and effective means for autonomous navigation and positioning of high orbit spacecraft. In the high dynamic environment, the carrier frequency, phase and pseudo code phase change greatly along with the supporter motion. Because the influence of Doppler frequency change introduced by supporter dynamics on pseudo code tracking loop can be eliminated by carrier assistance, the dynamic performance of receiver mainly depends on the carrier tracking module. The increase of propagation path and high dynamic signal of high orbit leads to problems of large loss of received signal path and weak signal of high orbit navigation receiver. Through carrying out special research on high orbit weak signal tracking technology, several simulations and analyses, reasonable design of loop noise bandwidth, adjustment of pre-integration time and other measures, the navigation weak signal of −173 dBw can be effectively and stably processed and traced. The algorithm has been applied to Chang'E-5 satellite, and provides technical guidance and index reference for deep space exploration projects, such as high orbit satellite navigation and circumlunar flying.

Keywords: High orbit spacecraft · Autonomous navigation · Weak signal · Loop · Integral time

1 Introduction

High earth orbit satellite includes geostationary orbit (GEO) satellite and highly eccentric orbit (HEO) satellites whose maximum orbit altitude is generally higher than 20,000 km. Currently, high orbit satellites are playing an increasingly important role in communication, navigation, meteorology, early warning and other fields. Autonomous navigation technology of high orbit spacecraft is one of new aerospace technologies needing to be developed urgently in China, and the use of navigation receivers in high orbit spacecraft has become the mainstream of engineering applications [1]. The biggest difference between the application of high orbit spacecraft navigation receivers and the terrestrial

R. Li et al. (Eds.): MOBILWARE 2022, LNICST 507, pp. 135–149, 2023.
https://doi.org/10.1007/978-3-031-34497-8_12

receivers is that the former needs to receive navigation satellite signals from the opposite side of the Earth. The increase in signal propagation path leads to the problem of large loss of path and weak received signal. Research on navigation with weak GPS signals started at the end of the 20th century and has been carried out on HEO, MEO, and GEO satellites for several on-orbit applications, verifying the availability of weak signals of sidelobes of GPS navigation satellites in high orbit [2, 3]. For example, the U.S. TEAMST-YES and Falcon Gold missions confirm that GEO transfer orbit satellites can successfully track GPS signals at an altitude of 26,000 km and send back GPS sampling data for ground processing; German Equator-S project operated in HEO orbit and successfully tracked the GPS sidelobe signal at an altitude of 61,000 km; in China, the GNSS high orbit receiver developed by Space Star Technology Company Limited was successfully applied to Chang'E-5 flight test vehicle, which completed GPS/GLONASS navigation signal reception and realized real-time navigation and positioning orbit determination algorithm in 50,000 km transfer orbit, and obtained high orbit GNSS signal characteristics with real-time orbit determination position accuracy of 15.8 m during 48 h continuous navigation tracking (3-axis, 1 σ). With the further development of navigation technology, China has realized the global network of Beidou-3 satellite navigation system. In order to adapt to the rapidly developing navigation market and the further demand of high orbit navigation tasks, it is necessary to carry out the research of high orbit GPS/BD2/GLONASS multi-system combined high-precision orbit determination [4–9] and its weak signal capture and tracking technology, among which the solution of long-term tracking without frequency loss is the key to stabilize the subsequent positioning algorithm.

The algorithm studied in this article is applied to the Chang'E-5 GNSS high orbit receiver. Based on the theory of weak signal tracking in high orbit and high dynamic environment, we analyze the loop tracking error and combine with the actual engineering application requirements, to simulate the weak signal tracking algorithm, verify the effectiveness of the algorithm, and derive the minimum limit of weak signal that can be tracked in the loop under the algorithm. In order to explore the application feasibility of the deep space navigation devices such as circumlunar flying, we conduct in-depth research on the combination of multiple systems, such as Beidou-3, GPS, GLONASS and other devices and carry out multi-fusion high orbit high precision navigation, so as to provide theoretical and engineering basis.

2 Tracking Principle of Weak Signal

There have been many studies on the principle of weak signal capture and tracking [10–15], among which, two processing methods based on the Square Root of Kalman Filter with inversion of unknown navigation bits have achieved better results in tracking weak signals [16].

Since the carrier tracking loop is the weak link of stand-alone receiver, its tracking threshold determines characteristics of the latter. The scheme of carrier pre-detection integrator, carrier discriminator and carrier filter determines characteristics of the receiver carrier tracking loop. Carrier loops are usually implemented using PLL (Phase Lock Loop, PLL) and FLL (Frequency Lock Loop, FLL). The three functions of pre-detection

integrator, discriminator and loop filter determine characteristics of the carrier loop. The characteristics of the carrier tracking loop of navigation receiver [17, 18] are shown in Fig. 1.

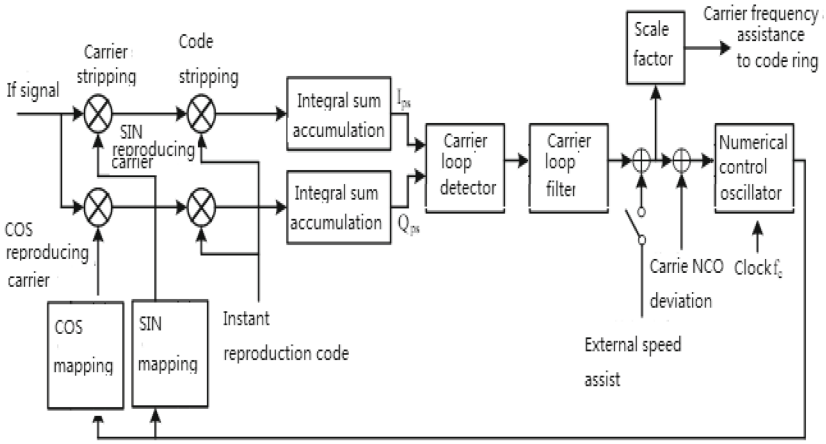

Fig. 1. Carrier tracking loop of navigation receiver

The Phase Lock Loop (PLL) aims to lock the phase of the input carrier signal. By adjusting the phase of the output signal, the phase between the output signal and the input signal can be consistent at all times [19, 20]. In practice, since the input to the PLL is not a continuous time signal, the corresponding PLL is in digital form. Considering the on-satellite dynamic effects, general onboard navigation receivers are mainly used in three-order PLL loop applications. The Costas loop has become a fairly common carrier loop for navigation receivers due to its insensitivity to 180° carrier phase shifts caused by data bit jumps.

When the discriminator of the PLL is used directly to discriminate the frequency difference between the input carrier and the copied carrier, the corresponding carrier loop becomes a frequency lock loop (FLL). Because the relative motion between the navigation satellite and the receiver causes Doppler shift, and the frequency drift of the receiver oscillator is unknown, the FLL needs to identify the frequency difference between the input carrier and the copied carrier, and adjust the copied carrier frequency output from the CNC oscillator accordingly, and achieve the same frequency with the input carrier after several adjustments. The FLL discriminator requires 2 samples in a data jump interval, and the maximum pre-detection integration time of FLL is 10 ms, and the ATAN2 discriminator is generally used as the discriminator in the case of low signal-to-noise ratio.

The main function of the code loop is to maintain the phase agreement between the copied C/A code and the received C/A code, and further to obtain the measurement of the received code phase as well as the pseudorange [21]. The settings of the programmable pre-detection integrator, code loop discriminator and code loop filter determine the characteristics of the receiver code tracking loop. During the operation of the receiver, the

code loop tracking module reproduces three receiver recurrent codes, advancing, immediate and lagging, which are correlated with the carrier stripped satellite signal, and the correlated signal is then integrated into the code loop discriminator, and the recurrent code is adjusted by the adjustment variables of the control CNC oscillator, so that the recurrent code is phase-aligned with the modulated PRN code of the received signal.

Similar to the carrier loop mechanism, the code loop uses a Delay Lock Loop (DLL), which can infer the phase of the received C/A code based on the control parameters of the copied C/A code or the code numerical control oscillator, etc. The DLL discriminator is smoothed to contain a non-zero mean noise floor, especially in the case of weak received signals, where accurate measurement of the noise floor becomes more important [22].

Generally, navigation receivers use PLL for carrier tracking. For dynamic environments, especially for satellite-based navigation receivers, there are large Doppler shifts and Doppler shift rates of change, mainly in the carrier tracking loops. To adapt to the satellite-based dynamic environment, the most effective method is to increase the loop noise bandwidth and reduce the pre-detection integration time. But, to reduce the effect of noise and improve the tracking accuracy, it is necessary to reduce the loop noise bandwidth and extend the pre-detection integration time (i.e., coherent integration time). To resolve the conflict, a compromise needs to be made in the design of the carrier loop [23]. In order to perform tracking of weak signals, it is necessary to simulate and analyze the tracking error of PLL, FLL and code loop, so as to design the tracking loop and code loop accordingly.

3 Error Analysis of Loop Tracking

3.1 Error Analysis of Phase Lock Loop (PLL)

The main sources of phase errors in the PLL circuit are phase jitter and dynamic stress errors. The phase jitter is the square root of the sum of the squares of the individual uncorrelated phase noise sources, which include thermal noise and oscillator noise, which in turn contains jitter caused by vibration and jitter caused by Allan Variance. Since the 3σ phase error caused by all noise sources should not exceed 450, the corresponding 1σ empirical method is to set the tracking threshold of the PLL to 150. In addition, other PLL jitter sources may be transient or negligible, so thermal noise is usually used as the only source of carrier tracking error. PLL thermal noise jitter is shown in Fig. 2.

As can be seen in Fig. 2(a), the PLL thermal noise jitter intensity is much smaller than the tracking threshold and flat under normal signal conditions ($C/N_0 \approx 44$ dB/Hz). As the carrier noise ratio decreases, the jitter intensity accelerates and the PLL tracking error becomes larger, making the tracking loop unstable. PLL thermal noise jitter is proportional to the square of the loop bandwidth and decreases with increasing cumulative summing time. Therefore, the PLL thermal noise jitter can be reduced by increasing the cumulative summing time and reducing the loop bandwidth. It should be noted that in a general signal tracking loop, the cumulative summing time is limited by the data code length, and reducing the loop bandwidth will compromise the dynamic performance of the loop.

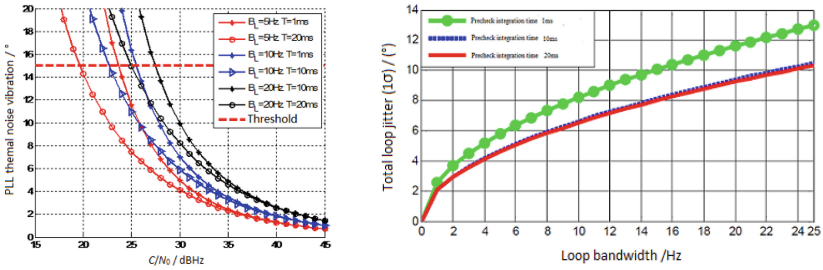

Fig. 2. Left (a): PLL thermal noise jitter, right (b): Relationship between PLL loop bandwidth and measurement error

Figure 2(b) shows the PLL loop jitter corresponding to different bandwidths at $C/N_0 = 29\text{dB/Hz}$, which can reflect the relationship between PLL loop bandwidth and measurement error.

Conduct simulation for the error of PLL tracking. Analysis of the simulation results in Fig. 2(b) shows that the pre-detection integration time of 1 ms, 10 ms and 20 ms can meet the requirement of total loop error less than 15° in the case of $C/N_0 = 29\text{dB/Hz}$ and jerk of 0 for the loop bandwidth from 0 to 18 Hz. The loop error of the pre-detection integration time of 20 ms is overall smaller than the loop error when the pre-detection integration time is 1ms, while the error of the pre-detection integration time of 10ms is not much different from the error of 20 ms.

3.2 Error Simulation and Analysis of Frequency Lock Loop (FLL)

Similar to PLL, the source of frequency measurement error of FLL also includes two parts: frequency jitter and dynamic stress error, where the frequency jitter is mainly caused by thermal noise, while the amount of frequency jitter caused by mechanical jitter and Allan Variance is neglected because it is relatively small [24]. Dynamic stress of FLL is much better at the same noise bandwidth and C/N_0. With reduced pre-detection integration time, dynamic stress performance of FLL will be improved to some extent. In addition, since the FLL discriminator requires two samples in one data jump interval, the maximum pre-detection integration time of FLL is 10 ms for C/A codes.

The main sources of FLL frequency errors are also thermal noise frequency jitter and dynamic stress errors. The effect of frequency jitter caused by base oscillator vibration and Allan Variance on FLL is small and negligible. For the FLL circuit, the empirical tracking threshold is that the jitter 3σ value caused by all loop stress sources is not allowed to exceed 90°within one pre-detection integration time t.

Figures 4 and 5 show the relationship curves of thermal noise jitter versus loop bandwidth for the same carrier noise ratio with different pre-detection times, and the relationship curves of thermal noise jitter versus loop bandwidth for the same pre-detection integration time with different carrier noise ratios, respectively.

As can be seen from Fig. 3, the thermal noise jitter of FLL is proportional to the loop bandwidth, inversely proportional to the pre-detection time and the carrier noise ratio, and independent of the spreading code rate and the loop filter order.

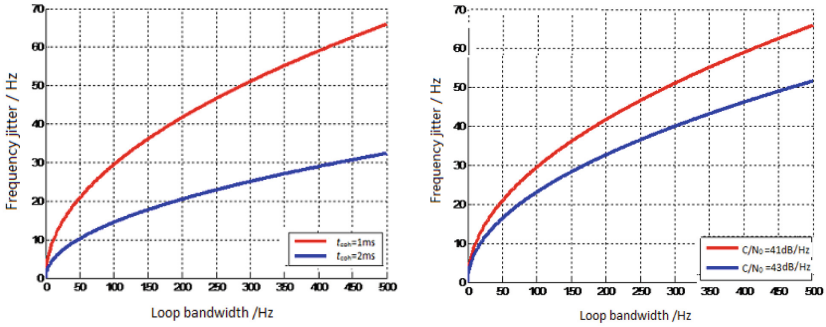

Fig. 3. Left(a): Thermal noise jitter under the same carrier noise ratio and different pre-detection time, right(b): Thermal noise jitter under the same pre-detection time and different carrier noise ratio.

Figure 4 shows the FLL loop jitter corresponding to different bandwidths at $C/N_0 = 29\text{dB/Hz}$, which can reflect the relationship between FLL loop bandwidth and measurement error.

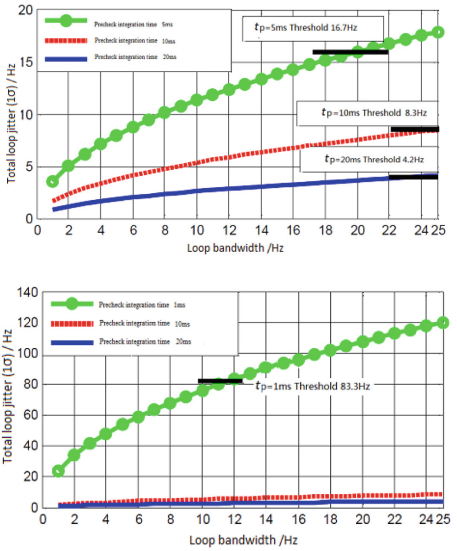

Fig. 4. Relationship between FLL loop bandwidth and measurement error, ($C/N_0 = 29\text{dB/Hz}$ Loop jitter corresponding to different bandwidths)

Analyzing the relationship between FLL loop bandwidth and measurement error, it can be seen that the FLL loop can meet the requirement that the total loop error is less than the corresponding threshold value in the case of C/and jerk of 0, pre-detection integration time of 1 ms, 10 ms and 20 ms in the case of loop bandwidth from 0 to 18 Hz.

In this case, the threshold value is calculated according to the FLL tracking threshold equation, i.e., $3\sigma_{FLL} = 3\sigma_{tFLL} + f_e \leq 0.25/t(Hz)$, where σ_{tFLL} is the thermal noise frequency jitter and f_e is the dynamic stress error in the FLL tracking loop. And the overall loop error for a pre-detection integration time t of 20 ms is smaller than the loop error for a pre-detection integration time t of 1ms.

3.3 Error Analysis of Delay Lock Loop (DLL)

Without considering multipath and other interferences, the sources of measurement errors in the code loop mainly include code phase jitter caused by thermal noise and dynamic stress errors. In the process of GPS software receiver code tracking (DLL), the main sources of error in ranging come from thermal noise distance error jitter and dynamic stress error. The DLL empirical method threshold is that the 3 σ value of jitter caused by all error sources in the loop is not allowed to exceed half of the linear traction range of the discriminator.

The carrier loop-assisted code tracking loop eliminates the effect of dynamic stress error, so as long as the carrier loop remains stable, the dynamic stress error experienced by the code loop is negligible, and only the thermal noise distance error jitter is considered in the code tracking threshold analysis. When the update time is 1ms, the thermal noise suppression performance of the second-order DLL with different parameters is shown in Fig. 5.

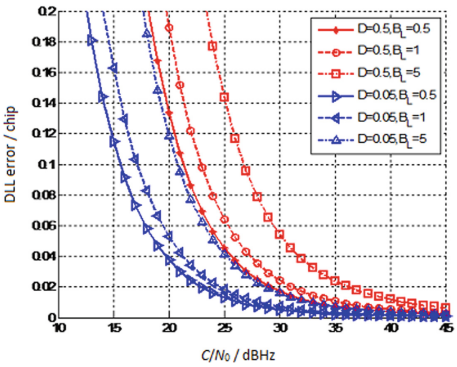

Fig. 5. Thermal noise suppression performance of second-order DLL (Loop update time = 1 ms)

It can be seen from Fig. 5: DLL thermal noise jitter increases at an accelerated rate as the carrier noise ratio decreases, making the tracking loop unstable. The DLL thermal noise jitter is proportional to the square of the loop bandwidth, and the thermal noise error becomes larger as the bandwidth is widened. Due to the carrier-assisted code technique, the dynamics in the code tracking loop are virtually removed, so the dynamic stresses experienced by the code loop are negligible as long as the carrier loop is kept stable, and this effect can be excluded from the code loop tracking threshold analysis.

Figure 6 shows the loop jitter corresponding to different code ring correlator intervals for $C/N_0 = 29\text{dB/Hz}$ and pre-detection integration time = 20 ms, which can reflect the relationship between the DLL loop bandwidth and the measurement error.

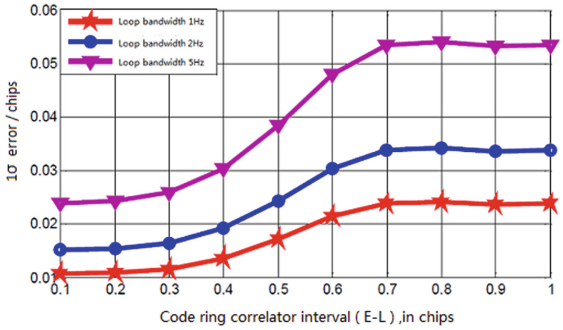

Fig. 6. Relationship between DLL loop bandwidth and measurement error, (C/N0 = 29 dB/Hz, Pre-detection integration time = 20 ms)

Analyzing the simulation results of DLL loop bandwidth and measurement error, it can be seen that DLL can meet the requirements of total loop error in the case of loop bandwidth from 0 to 18 Hz when C/N0 = 29 dB/Hz and pre-detection integration time is 20 ms, while different code loop correlator interval DLL loop error is different.

4 Simulation of Weak Signal Tracking Algorithm

4.1 Simulation Scheme for Weak Signal Tracking

Weak GNSS signal tracking and processing techniques focus on the design of frequency discriminator, phase discriminator, loop filter, etc. After considering capturing and removing the NH code phase, the tracking loop processing technology is not much different for BD-2 B1 and GPS L1 C/A codes, and the loop parameter indexes applicable to GPS can also meet the requirements of BD-2. The following are the simulation results corresponding to each loop.

The trace processing loop simulink verification platform is shown in Fig. 7.

The tracking parameter switches are mainly based on the carrier noise ratio. GPS tracking parameters switching conditions (parameters of each satellite are controlled independently) are as follows: the first set of parameters (PLL coherent integration time of 2 ms, code loop coherent integration time of 2 ms, FLL coherent integration time of 1ms, FLL bandwidth of 0.3, code loop bandwidth of 2) is used after switching from capturing channel to tracking channel. When the tracking time is greater than 1,000 ms, it is switched to the second set of parameters (PLL coherent integration time of 10 ms, code loop coherent integration time of 10 ms, FLL coherent integration time of 5 ms, FLL bandwidth of 0.4, code loop bandwidth of 0.6). When the second set of parameters is tracked for more than 500 ms and the carrier noise ratio is greater than 23, it is switched to the third set of parameters (PLL coherent integration time of 20 ms, code loop coherent integration time of 20 ms, FLL coherent integration time of 10 ms, PLL bandwidth of 8, code loop bandwidth of 1). Check the carrier noise ratio status every 0.5s under the third set of parameters tracking status, and cut back to the second set of parameters when the carrier noise ratio status is less than 20.

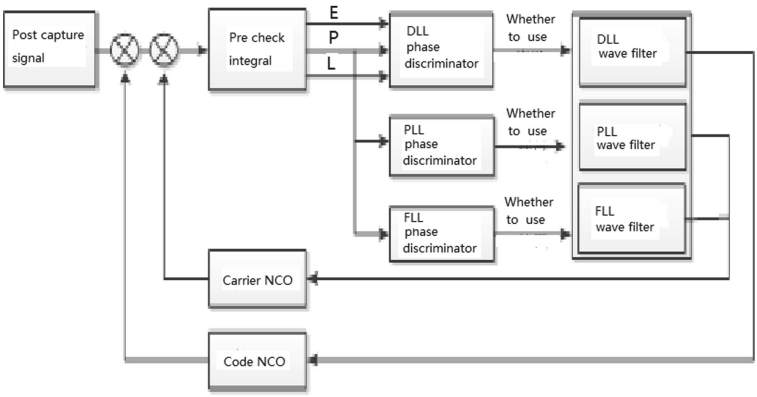

Fig. 7. Weak signal tracking loop

BD tracking parameters switching conditions (parameters of each satellite are controlled independently) are as follows: the first set of parameters (PLL coherent integration time of 1ms, code loop coherent integration time of 1ms, FLL coherent integration time of 0.5 ms, FLL bandwidth of 0.3, code loop bandwidth of 2) is used after switching from capturing channel to tracking channel. When the tracking time is greater than 1,500 ms, it is switched to the second set of parameters (PLL coherent integration time of 2 ms, code loop coherent integration time of 2 ms, FLL coherent integration time of 1ms, FLL bandwidth of 0.2, code loop bandwidth of 0.5). When the second set of parameters is tracked for more than 1,000 ms and the carrier noise ratio is greater than 22, it is switched to the third set of parameters (PLL coherent integration time of 2 ms, code loop coherent integration time of 2 ms, FLL coherent integration time of 1ms, PLL bandwidth of 14, code loop bandwidth of 0.5). Check the carrier noise ratio status every 0.5 s under the third set of parameters tracking status, and cut back to the second set of parameters when the carrier noise ratio status is less than 20. If it is less than or equal to 30 for 20 s consecutively, it switches to the fourth set of parameters (PLL coherent integration time of 2 ms, code loop coherent integration time of 2 ms, FLL coherent integration time of 1ms, PLL bandwidth of 6, code loop bandwidth of 0.5), whose tracking sensitivity is higher than the third set.

4.2 Simulation Results of Dynamic Environment

Use Matlab simulink to simulate the GPS receiver tracking loop. Figure 8 shows the top-level structure of the simulation system. The simulation system uses frame processing for the simulation of signal data.

Considering that the dynamic effect of code loop tracking has been removed from the carrier tracking loop, the simulation is actually the weak signal DLL tracking accuracy when the dynamics is 0. Select the code loop discriminator type $(I_E - I_L) \times I_P + (Q_E - Q_L) \times Q_P$ and verify the loop tracking performance corresponding to different loop bandwidths and integration times under different C/N_0 conditions.

According to the analysis of the in-satellite dynamic range of the L1-band GPS satellites received by HEO and GEO, the velocity range is ±10 km·s-1 and the acceleration

range is ±2 g, which corresponds to the Doppler shift range ± 53 kHz and the Doppler shift change rate ±105 Hz·s-1. Taking −175 dBw as an example, the corresponding PLL and DLL tracking performance at −175 dBw (C/N0 = 29 dB/Hz) to −170 dBw (C/N0 = 34 dB/Hz) is determined by analyzing the corresponding loop tracking parameters, including loop tracking bandwidth Bn, loop pre-detection integration time tp, as shown in Figs. 8, 9 and 10.

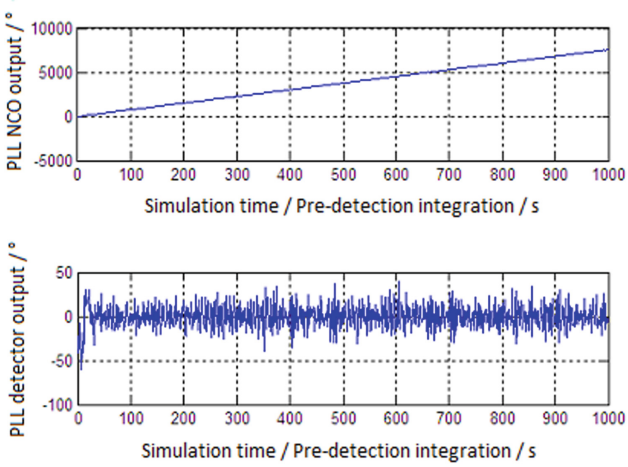

Fig. 8. Figure 10 PLL tracking performance at BnPLL = 15 Hz, t_p = 20 ms, (C/N_0=29 dB/Hz, B_n=15 Hz, Total simulation times = 1000,Correlation operation time = 20 ms, Statistics start from the 200th per detection integration cycle, σ_{PLL} (sim) = 12.261

Statistics of theoretical and simulated values of tracking loop error in dynamic environment (acceleration 2g) are performed for the loop parameters used in the above simulation. As for the BD-3 GEO satellite, its data bit rate is 500 bit·s-1, which cannot be integrated coherently for a long time and requires a non-coherent carrier loop and a non-coherent code loop, which will not be discussed too much here. The simulation analysis results are shown in Table 1.

According to the simulation results, it can be seen that PLL and DLL can complete tracking normally under pre-detection integration time of 20 ms and acceleration of 2 g, the pseudo-range measurement error is within 15m at −175 dBw, and the carrier phase measurement accuracy is about 10°.

Statistics on the GPS L1 signal power received by GEO and the corresponding reception altitude angle show that the maximum received power at GEO is about −163 dBw and the receiver sensitivity is −182 dBw, a difference of 19 dB, so there is a certain degree of mutual interference between strong and weak signals in the navigation signal processing. Similarly, the comparison between the received power of HEO orbit and the received altitude angle shows that the maximum received power of HEO is also about −163 dBw, which is more than 20 dB different from the lowest received power. Therefore, when dealing with weak signals for high-orbit navigation (−175 dBw), it is

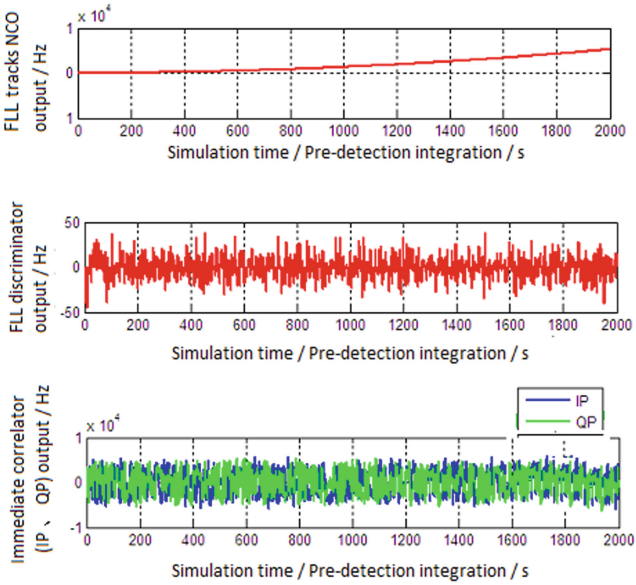

Fig. 9. FLL tracking performance at BnFLL = 10 Hz, t_p = 5 ms, (C/N_0=29 dB/Hz, B_n=10 Hz, Total simulation times = 1000, Correlation operation time = 5ms, Statistics start from the 500th per detection integration cycle, σ_{FLL} (sim) = 9.1251 Hz, σ_{FLL} (theory) = 7.9918 Hz)

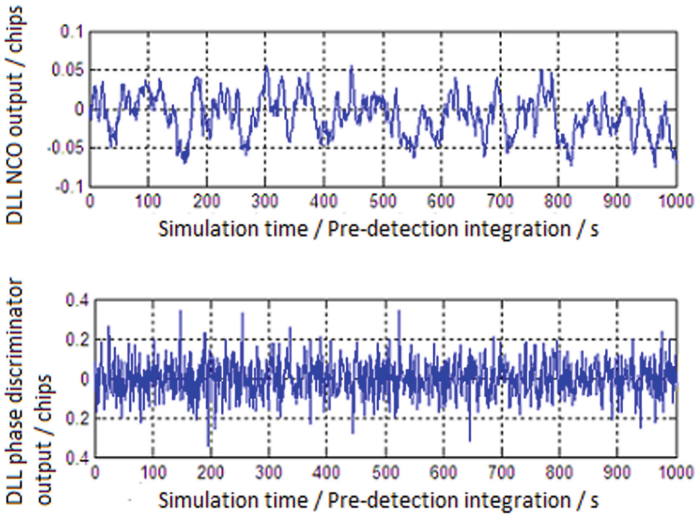

Fig. 10. DLL tracking performance when BnFLL = 2 Hz, t_p = 20 ms, (C/N_0=29dB/Hz,Δ = 1chips, B_n=2 Hz, Total simulation times = 1000, Statistics start from the 50th per detection integration cycle, σ_{DLL} (sim) = 0.043864chips, σ_{DLL} (theory) = 0.035003chips)

Table 1. Simulation analysis of weak signal loop tracking performance

Loop Type	Receiving Power/dBw	Loop Bandwidth/Hz	Pre-detection integration time/ms	Theoretical value	Simulation error
PLL	−160	31.38	1	2.05°	2.07°
	−170	15	1	4.45°	5.67°
	−171	15	20	4.99°	6.91°
	−172	15	20	5.62°	7.13°
	−173	15	20	6.32°	8.56°
	−174	15	20	7.10°	9.78°
	−175	15	20	7.99°	11.68°
FLL	−160	21.2	1	9.42 Hz	9.84 Hz
	−170	10	5	4.17 Hz	4.88 Hz
	−171	10	5	4.72 Hz	5.59 Hz
	−172	10	5	5.36 Hz	6.42 Hz
	−173	10	5	6.10 Hz	7.14 Hz
	−174	10	5	6.97 Hz	7.83 Hz
	−175	10	5	7.99 Hz	9.12 Hz
DLL	−160	1.06	20	1.37 m	1.69 m
	−170	2	20	5.67 m	6.22 M
	−171	2	20	6.40 m	7.44 m
	−172	2	20	7.22 m	7.99 m
	−173	2	20	8.17 m	9.19 m
	−174	2	20	9.25 m	9.73 m
	−175	2	20	11.29 m	13.15 m

also necessary to consider the phenomenon of channels interfering with each other due to the simultaneous reception of signals of higher power.

According to the simulation results, when the signal power difference is within 20 dBw, the signal can find out the relevant peak normally. When the difference between the two signal powers is more than 20 dBw, it will have an impact on the correlation peak of the signal, which may mistakenly treat the interdependent peak as the self-correlation peak, resulting in the wrong capture of the signal. The method has been proven in engineering to identify loop mis-capture tracking by demodulating the messages to distinguish between strong and weak signals.

4.3 Real-Time Orbit Determination Results

By applying the above technologies to engineering practice, the real-time orbit determination accuracy of Chang'E-5 satellite can reach 15.81 m. By sending the raw observation data downlinked from GNSS to the third party for post-event orbit calculation, and differencing the real-time bit velocity in the real-time orbit determination state in telemetry with the calculated orbit, we obtain the real-time orbit determination error, which is used to evaluate the GNSS on-orbit performance. The analysis period of the raw observation data is about 48 h. The specific conclusions are as follows: GNSS position error of the orbit determination is 15.8133 m (tri-axis, 1σ), as shown in Fig. 11(a); velocity error is 0.012108 m·s-1 (tri-axis, 1σ), as shown in Fig. 11(b).

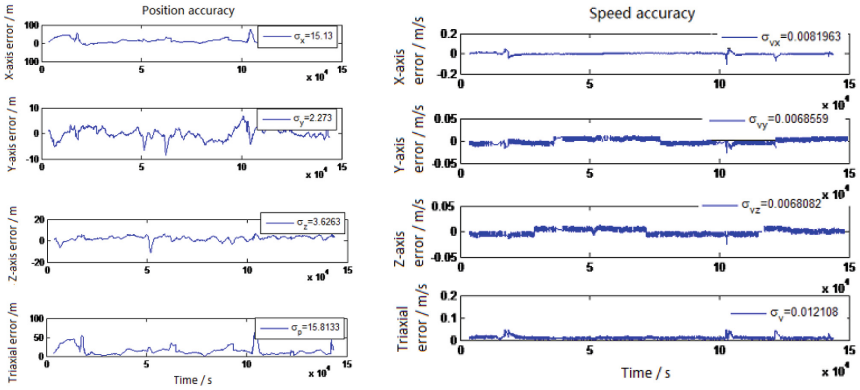

Fig. 11. Left(a): Position accuracy of the high orbit navigation receiver, right(b): Speed accuracy of the high orbit navigation receiver.

5 Conclusion

Based on the analysis of the velocity and acceleration of relative motion, it is known that the relative velocity range of the high-orbiting satellite-based navigation receiver is ±10 km·s-1 and the relative acceleration range is ±2 g, which corresponds to the Doppler shift range ±53 kHz and the Doppler shift change rate ±105 Hz·s-1. The analysis of GEO and HEO received power and received altitude angle shows that the maximum power of high orbit received GPS signal with antenna gain is −153 dBw, and it is almost able to receive the signal of the main lobe, the first sidelobe and the second sidelobe when the received power is −173 dBw.

Weak signal tracking theoretical analysis and simulation results show that the algorithm enables the receiver to handle −173 dBw navigation weak signals stably in high-orbit orbit applications, and the research results can provide theoretical support and technical index reference for real-time orbit determination of high-orbit satellites in orbit, and enhance the autonomy and real-time performance of high-orbit satellites. We will further expand the scope of simulation tests to verify the structure, conduct error

analysis considering other parameters and carry out physical tests to further explore the feasibility of the application of navigation equipment in deep space such as circumlunar flying, study the feasibility of combined navigation of Beidou-2 navigation system and other navigation systems in high orbit environment, and lay the theoretical and engineering foundation for multi-fusion high orbit high precision combined navigation of high orbit navigation receivers and other equipment such as INS.

References

1. Jiang, H.: Acquisition of Beidou Weak Signal in High Orbit Environment. Hebei University of Science and Technology, Shijiazhuang (2017)
2. Winternitz, L.M.B., Bamford, W.A., Heckler, G.W.: A GPS receiver for high-altitude satellite navigation. IEEE J. Sel. Top. Signal Process. **3**(4), 541–556 (2009)
3. Unwin, M., De Vos Van Steenwijk, R., Blunt, P., et al.: Navigating above the GPS constellation – preliminary results from the SGR-GEO on GIOVE-A. In: Proceedings of the 26th International Technical Meeting of the Satellite Division of The Institute of Navigation, pp. 3305–3315. ION, Nashville (2013)
4. Guo, R., Liu, L., Li, X., et al.: Precise orbit determination for GEO satellites based on both satellite clock offsets and station clock offsets. Chinese J. Space Sci. **32**(3), 405–411 (2012)
5. Liang, M., Qin, H., Li, F.: Solving the near-far problem for positioning the high earth orbital satellite with GPS. Chinese J. Space Sci. **30**(3), 255–262 (2010)
6. Li, J., Ma, G.: Effect of ionospheric irregularities on GPS performance. Chinese J. Space Sci. **33**(2), 158–169 (2013)
7. Ji, S., Zhu, W., Xiong, Y.: Calculate and application of the GPS satellite clock offset. Chinese J. Space Sci. **21**(1), 42–48 (2001)
8. Liu, H., Wang, H.: Orbit determination of satellite on the Middle-high earth orbit based on GPS. Chinese J. Space Sci. **25**(4), 293–297 (2005)
9. Li, L., Li, C., Huang, W., Zhou, Y.: Orbit determined method of high elliptical orbit satellite based on BDS navigation and inter-satellite link. Chinese J. Space Sci. **38**(6), 915 (2018). https://doi.org/10.11728/cjss2018.06.915
10. Wu, Y.: Research on Acquisition and Tracking Algorithms for GPS Weak Signal. Chongqing University, Chongqing (2012)
11. Wie, J.: Research on Acquisition and Tracking of GPS Weak Signals under Multipath Interference. Nanjing University of Aeronautics and Astronautics, Nanjing (2014)
12. Qiu, L., Li, L.: GPS signal acquisition based on FFT. In: 2010 Second International Conference on Information Technology and Computer Science, pp. 110–113. IEEE, Kiev, Ukraine (2010). https://doi.org/10.1109/ITCS.2010.33
13. Liu, Y., Chen, Z., Guo, S.: Implement and performance analysis of pseudo code acquisition based on FFT. In: Proceedings of the 5th World Congress on Intelligent Control and Automation. Hangzhou, China (2004)
14. Dong, Z., Wu, S.: New acquisition method for DSSS with large Doppler. Syst. Eng. Electron. **30**(8), 1424–1426 (2008)
15. Hu, H., Sun, H., Ji, Z.: Study on algorithm and control strategies of GPS carrier tracking loop under high dynamic conditiong. J. Astronaut. **32**(8), 1805–1812 (2011)
16. Zhou, G.: Research and Realization of Acquisition and Tracking for Weak GPS Signals. Shanghai Jiao Tong University, Shanghai (2009)
17. Liu, W., Yuan, H., Wei, D., et al.: A new GNSS signal carrier tracking algorithm for ionospheric TEC monitoring. Chinese J. Space Sci. **34**(1), 63–72 (2014)
18. Tang, L.: Research on the Tracking Technology in GNSS. Xidian University, Xi'an (2017)

19. Song, C., Wang, X., Zhuan, Z.: Estimate algorithm for pseudo-code phase delay and its uncertainty in the assisted GPS receiver. Chinese J. Space Sci. **29**(6), 620 (2009). https://doi.org/10.11728/cjss2009.06.620
20. Wang, W.: Research on Beidou Navigation Signal Tracking Algorithms and Software Implemention. Xidian University, Xi'an (2017)
21. Hong, Y., Yao, Z., Lu, M.: Research on adaptability of satellite navigation signal code tracking theory. Comput. Simul. **29**(12), 53–56, 375 (2012)
22. Yu, Y.: Research and Implementation of GNSS Signal Tracking Technology for High-Orbit Spacecraft. Dalian University of Technology, Dalian (2018)
23. Li, Y.: Research and Implement of the Acquisition and Tracking for the New-styled Navigation Signals. National University of Defense Technology, Changsha (2013)
24. Wen, C., Yue, F., Qiu, Y., et al.: Research on tracking of high earth orbit BDS weak signal. J. Spacecraft TT&C Technol. **32**(4), 363–370 (2013)